Volume 19 | Number 12 | 28 March 2017 | Pages 1573–1692

CrystEngComm

rsc.li/crystengcomm

ROYAL SOCIETY OF CHEMISTRY

PAPER

Lili Fan, Ming Xue *et al.*

In situ confinement of free linkers within a stable MOF membrane for highly improved gas separation properties

CrystEngComm

PAPER

View Article Online
View Journal | View Issue

Cite this: *CrystEngComm*, 2017, **19**, 1601

Received 14th January 2017,
Accepted 8th February 2017

DOI: 10.1039/c7ce00102a

rsc.li/crystengcomm

Published on 09 February 2017. Downloaded on 21/03/2017 02:01:20.

In situ confinement of free linkers within a stable MOF membrane for highly improved gas separation properties†

Zixi Kang,[a] Lili Fan,*[a] Sasa Wang,[a] Daofeng Sun,[a] Ming Xue*[b] and Shilun Qiu[b]

A stable MOF membrane with guest molecules encapsulated in the pores by *in situ* synthesis has been successfully fabricated. The *in situ* confinement of linkers in the channels of the MOF membrane improves its gas separation properties, which may provide a general method for fine-tuning the pore size of MOF membranes and develop the functional applications of porous MOF materials.

Introduction

As an emerging class of porous crystalline materials, metal–organic frameworks (MOFs) have received great attention in gas storage and separation research.[1–11] Separation of mixtures is a critical process in the chemical industry, accounting for around half the total energy use in the industry.[12] Mixtures of gases with similar molecular sizes or physical properties are particularly difficult to separate.[13] Gas separation based on membranes, which has undergone rapid development over the past few decades, possesses the advantages of having high efficiency, reduced carbon footprint and easy operation, and shows promise as a technique for addressing energy-use and environmental challenges.[14–20] As the core of the membrane separation process, membrane materials including polymers and zeolites have been extensively investigated.[21,22] Polymers are the most widely used membrane materials in the practical field of gas separation owing to their advantages such as ease of processing and low cost. However, due to their wide pore-size range, most polymer membranes cannot achieve ideal permeability and selectivity at the same time.[23,24] The uniform pore-size distribution of zeolite membranes allows them to overcome the disadvantages of polymer membranes and provide simultaneously high permeability and selectivity. The limitation of structures and high cost of production restrict the application of zeolite membranes in gas separation.[25,26]

MOFs can be made into effective membranes for gas separation due to the tailorability of their pore structure by varying the ligands and metal centers.[27–34] One of the most striking features of MOFs is that their nanospace can provide ideal room to accommodate guest molecules, and the resulting "guest@MOFs" can serve as platforms for host–guest chemistry studies.[35–37] Recent studies have reported that the pore size of MOF membranes can be adjusted effectively by introducing guest molecules into their channels. This strategy was originally used in zeolite membranes for fine-tuning the pore size of the LTA-type membrane by ion-exchange.[38,39] As for the MOF membrane, Caro *et al.* developed a covalent post-functionalization strategy to modify ZIF-90 to enhance its hydrogen selectivity.[40] The post-functionalization strategy was not only helpful in eliminating intercrystalline defects but also constricted the pore aperture, giving an improved molecular sieving performance for gas separation. The same group also reported that the gas separation performance of the MOF-74 membrane could be enhanced by modification of ethylenediamine into the framework.[41] In these cases, guest molecules were assembled in the pores of MOF frameworks to improve their gas separation properties by post-functional processes, which usually require steps additional to the synthesis. Our strategy is to tailor the pore size of the MOF membrane *in situ*, while keeping the original guest molecules in the structure. We have found a parent MOF $[Ni_2(L\text{-asp})_2(bipy)]$ (L-asp = L-aspartic acid, bipy = 4,4′-bipyridine) to be particularly interesting.[42] Its membrane has been examined for gas separation and chiral resolution.[28,43] During our studies on confining guest molecules in the pores of MOF membranes to tailor their molecular sieving properties, we observed that the bpe (1,2-bis(4-pyridyl)ethylene) pillar linker had the same connectivity as the bipy ligand in constructing the isostructural $[Ni_2(L\text{-asp})_2(bpe)]\cdot(G)$ framework (G = guest), which permanently confined the excess bpe ligand in the channels.[44] In this study, the MOF $[Ni_2(L\text{-asp})_2(bpe)]\cdot(G)$ was selected as a "proof of concept" model to prepare a high-quality and continuously

[a] *College of Science, China University of Petroleum (East China), Qingdao, Shandong, 266580, People's Republic of China. E-mail: lilifan@upc.edu.cn*
[b] *State Key Laboratory of Inorganic Synthesis and Preparative Chemistry, Jilin University, Changchun, 130012, P. R. China. E-mail: xueming@jlu.edu.cn*

† Electronic supplementary information (ESI) available. See DOI: 10.1039/c7ce00102a

Published on 09 February 2017. Downloaded on 21/03/2017 02:01:20.

grown membrane. The guest molecules were encapsulated in the pores during the membrane fabrication step with better dispersion. The $[Ni_2(L\text{-asp})_2(bpe)]\cdot(G)$ membrane showed a significantly enhanced gas separation performance with a H_2 permeance of 1.02×10^{-6} mol m^{-2} s^{-1} Pa^{-1} and a H_2/CO_2 selectivity of 24.3 due to the *in situ* guest molecules.

Experimental

Materials

Nickel carbonate ($NiCO_3$, analytical grade), methanol, L-asp, and the bidentate aromatic nitrogen donor bpe were used as-received. Nickel meshes (180 mesh, Xinxiang City, 540 Equipment Co., China) were used as the membrane support. The nickel net was first cut into circular wafers (10 mm in diameter). Then, they were washed with ethanol and deionized water under ultrasonication to clean the surface. Finally, these wafers were dried in an oven at 100 °C for 5 hours at least.

Preparation of Ni(L-asp)$(H_2O)_2\cdot H_2O$ (Ni(L-asp))

L-Asp (2.63 g, 0.02 mol) was first dissolved in a certain amount of water. When this solution was heated to 100 °C, $NiCO_3$ (2.86 g, 0.024 mol) was added. The final solution was evaporated at 100 °C to prepare the Ni(L-asp) powders.

Preparation of the $[Ni_2(L\text{-asp})_2(bpe)]\cdot(G)$ membrane on nickel mesh

0.1 g (0.75 mmol) of L-asp was dissolved in a mixture containing 2 mL of methanol (62.4 mmol) and 0.2 mL of water (11.1 mmol). To this solution, 0.068 g of bpe (0.375 mmol) was added and stirred for 1 hour. A nickel mesh and the final mixture with a composition of 1.0L-asp : 0.5bpe : $15H_2O$: $83CH_3OH$ were sealed into an autoclave and heated at 150 °C for 24 hours. After this process, a seed layer was grown on the surface of the nickel mesh. Then, the seeded nickel mesh was placed vertically in a Teflon-lined autoclave, in which the composition of the reaction solution was 1.0bpe : 0.9Ni(L-asp) : $333H_2O$: $263CH_3OH$, for secondary growth at 150 °C for 2 days. Finally, the membrane was taken out, washed with CH_3OH and H_2O, and dried at 80 °C. The membrane was activated at 150 °C in air for 10 hours.

Characterization

The crystalline structures of the membranes on nickel nets before and after activation were determined by powder X-ray diffraction (PXRD) measurements using a SHIMAZU LabX XRD-6000 X-ray diffractometer with Cu Kα radiation (λ = 1.5418 Å). The macroscopic and microscopic features of these $[Ni_2(L\text{-asp})_2(bpe)]\cdot(G)$ membranes on nickel nets were characterized using an optical microscope (Leica DM 2500P) and an analytical scanning electron microscope (JEOS JSM-6510A), respectively. Gas adsorption–desorption measurements of H_2 (99.995%), CO_2 (99.995%), CH_4 (99.95%) and N_2 (99.995%) on MOF powder samples were carried out on an Autosorb iQ2 adsorptometer from Quantachrome Instruments. The sample was degassed at 423 K overnight under vacuum, and the measurements were carried out at 273 K and 298 K. For the experimental setup of gas-separation measurement, the membrane was set in a stainless steel cell at room temperature and standard atmospheric pressure. One side of the membrane was swept by argon while the other side was exposed to single gases or gas mixtures. A soap-film flow meter was used to measure the flux of the gas. The volume ratio of the gases in the binary mixture was 1 : 1 and the gas that penetrated the membrane was analyzed using a gas chromatograph (SHIMADZU GC-2014C).

The permeability which is termed the permeance[45] (P_i (mol m^{-2} s^{-1} Pa^{-1})) of the MOF membrane was calculated using the following eqn (1):

$$P_i = \frac{N_i}{\Delta p_i \times A} \quad (1)$$

where N_i (mol s^{-1}) is the permeate flow rate of component i, Δp_i (Pa) is the trans-membrane pressure drop of i, and A (m^2) is the membrane area.

The membrane permselectivity was evaluated using a separation factor ($\alpha_{i,j}$),[45] which was obtained according to eqn (2):

$$\alpha_{i/j} = \frac{X_i/X_j}{Y_i/Y_j} \quad (2)$$

where i and j represent the two components in the mixture, and X and Y are the mole fractions in the permeate and feed solution, respectively.

Results and discussion

Preparation of the $[Ni_2(L\text{-asp})_2(bpe)]\cdot(G)$ membrane

In $[Ni_2(L\text{-asp})_2(bpe)]\cdot(G)$, as the "extended ligand," the longer bpe linker is expanded by 2.5 Å compared with the distance in the parent compound. It shows a slight distortion from the parent orthorhombic structure, and has a similar window cross section of 4.1 × 3.9 Å and a pore cross section of 7.8 × 3.3 Å. As shown in Fig. 1a and b, the bpe molecules are present with overlapping components along the *a* axis, which leads to the formation of narrow windows in the structure. The void volume of $[Ni_2(L\text{-asp})_2(bpe)]\cdot(G)$ is 24.8% of the total volume. Elemental analysis was carried out on the powder scraped from the membrane, and the result confirmed the formula of $[Ni_2(L\text{-asp})_2(bpe)][(bpe)_{0.4}(H_2O)$, which is consistent with the MOF crystal.[44] The bpe amount in the structure remains unchanged after heating to 100 °C, vacuum treatment and even Soxhlet extraction, suggesting that the guest molecule bpe is stable in the framework.

A seeding secondary growth process was applied to prepare an inter-grown $[Ni_2(L\text{-asp})_2(bpe)]\cdot(G)$ membrane for gas separation (Scheme 1). The nickel mesh acts as the only metal source for releasing nickel ions coordinated with

 This journal is © The Royal Society of Chemistry 2017

Published on 09 February 2017. Downloaded on 21/03/2017 02:01:20.

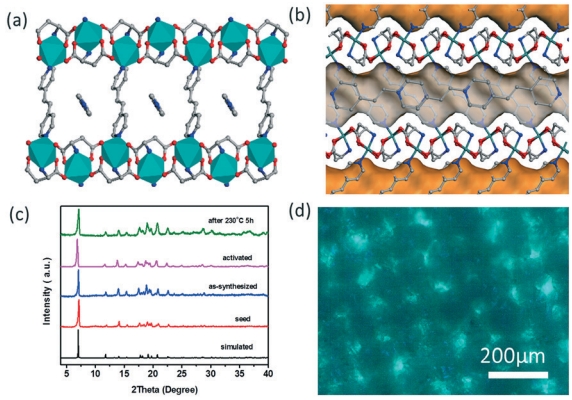

Fig. 1 (a) 3D structure of $[Ni_2(L\text{-asp})_2(bpe)]\cdot(G)$ with guest molecules of bpe, viewed along the *c* axis. (b) 3D structure of $[Ni_2(L\text{-asp})_2(bpe)]\cdot(G)$ with the corrugated channels filled with excess bpe linkers (Ni cyan, C gray, N blue, O red; H atoms are omitted for clarity). (c) PXRD patterns of the simulated, seed layer, as-synthesized, activated and heat-treated $[Ni_2(L\text{-asp})_2(bpe)]\cdot(G)$ membranes; (d) optical micrograph of the $[Ni_2(L\text{-asp})_2(bpe)]\cdot(G)$ membrane surface.

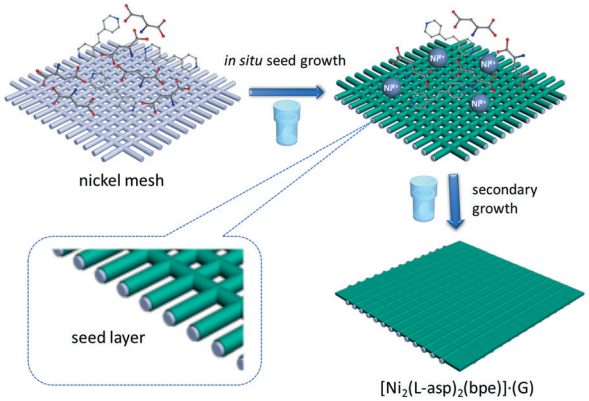

Scheme 1 Preparation process of the $[Ni_2(L\text{-asp})_2(bpe)]\cdot(G)$ membrane.

ligands to form a seed layer, after which a second growth process is carried out to give a well inter-grown MOF membrane.

The PXRD patterns collected for the seed layer and $[Ni_2(L\text{-asp})_2(bpe)]\cdot(G)$ membrane are shown in Fig. 1c. As can be seen, the seeded layers are composed of crystalline particles and free of impurities. The PXRD pattern of the $[Ni_2(L\text{-asp})_2(bpe)]\cdot(G)$ membrane is in accordance with the simulated pattern, suggesting that highly crystalline MOF crystals were grown on the support surface. To examine its thermal stability, the $[Ni_2(L\text{-asp})_2(bpe)]\cdot(G)$ membrane was kept in an oven at 235 °C for 5 hours under air atmosphere. The corresponding PXRD pattern reveals that the membrane maintained its crystalline structure. We can also see from the TGA curve that the $[Ni_2(L\text{-asp})_2(bpe)]\cdot(G)$ MOF maintains its crystal structure including the guest bpe up to 300 °C, indicating that the membrane has the desired thermal stability (Fig. S1†).

The optical micrograph of the nickel mesh-supported $[Ni_2(L\text{-asp})_2(bpe)]\cdot(G)$ membrane shown in Fig. 1d indicates that the nickel mesh acts as a homogeneous support allowing the continuous formation of the membrane over a large area. The morphology of the $[Ni_2(L\text{-asp})_2(bpe)]\cdot(G)$ seed layer and the membrane are shown in SEM images (Fig. 2 and Fig. S2†). It can be observed from Fig. 2a and Fig. S2† that the seed crystals homogeneously cover the support surface and form a continuous layer with a roughness comparable with the crystal size. The nickel mesh was the only Ni source for the synthesis of the seed layer. This helps to build a strong interaction between the seed layer and nickel mesh support and obtain a seed layer with uniform distribution, which is of paramount importance for the fabrication of a continuous and defect-free membrane because the seeds promote uniform membrane growth on the entire support surface. A secondary growth of the seed layer was subsequently carried out with the addition of nickel salt. From Fig. 2b–d and Fig. S2c and d,† it can be observed that a continuous and high-quality $[Ni_2(L\text{-asp})_2(bpe)]\cdot(G)$ membrane formed on the surface of the nickel mesh. The crystals in the membrane were well inter-grown and tightly connected with the threads of the nickel mesh with a thickness of 20–30 μm. The above characterization suggests that a structurally stable and large-area continuous MOF membrane was successfully fabricated by a simple secondary growth method.

Gas adsorption and separation on the $[Ni_2(L\text{-asp})_2(bpe)]\cdot(G)$ membrane

As shown in the gas adsorption isotherms of the $[Ni_2(L\text{-asp})_2(bpe)]\cdot(G)$ membrane (Fig. S3†), the uptake of all the gases was fairly small, corresponding to the narrow channels. The relatively high adsorption amount of CO_2 in the membrane is due to the electrostatic interaction between CO_2 molecules and the bpe ligands.[55] The low H_2 uptake can be attributed to a lower affinity for H_2 molecules. These results

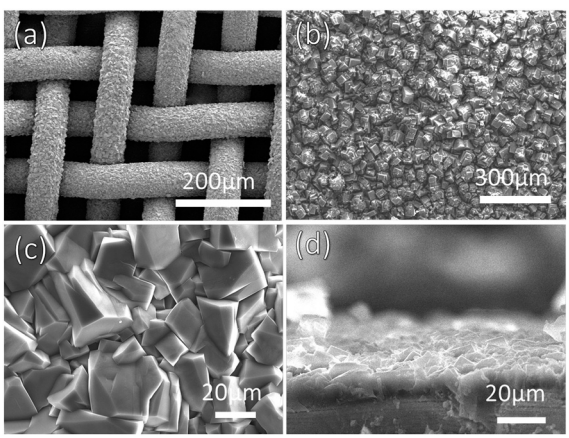

Fig. 2 (a) SEM image of the seeded nickel mesh; (b and c) top view and (d) cross-section SEM images of the $[Ni_2(L\text{-asp})_2(bpe)]\cdot(G)$ membrane.

Published on 09 February 2017. Downloaded on 21/03/2017 02:01:20.

Table 1 Mixture gas permeances and separation factors for the $[Ni_2(L\text{-}asp)_2(bpe)]\cdot(G)$ membrane at 25 °C and 1×10^5 Pa

Gas	H_2	CO_2	H_2	N_2	H_2	CH_4
Permeance $\times 10^{-7}$ (mol m^{-2} s^{-1} Pa^{-1})	10.2	0.452	10.0	0.837	10.0	1.29
S.F.	24.3		12.1		7.77	
Ideal S.F.	6.5		9.3		14	

suggest that the $[Ni_2(L\text{-}asp)_2(bpe)]\cdot(G)$ membrane has a great ability to resolve H_2 from other gases.

Following the successful construction of the $[Ni_2(L\text{-}asp)_2(bpe)]\cdot(G)$ membrane, the gas permeation performance was investigated for the single gases H_2, N_2, CO_2 and CH_4 and the binary gas mixtures H_2–N_2, H_2–CO_2 and H_2–CH_4 with equal volume ratios. The calculated gas permeances and separation factors are presented in Table 1. In the single gas permeation tests (Fig. 3a), the H_2 permeation flux was much higher than those of the other gases. Ideal separation factors were remarkably enhanced and the gas permeances slightly decreased compared with our previously reported $Ni_2(L\text{-}asp)_2(bipy)$ membrane ($P_{H_2} = 2.38 \times 10^{-6}$ mol m^{-2} s^{-1} Pa^{-1}, $H_2/CO_2 = 10.2$),[28] which can be attributed to the different pore structures of these two MOFs. Although the pore size of $[Ni_2(L\text{-}asp)_2(bpe)]\cdot(G)$ is a little larger than that of $Ni_2(L\text{-}asp)_2(bipy)$ as the molecular size of bpe is larger than that of bipy, the guest disorder in the channels of $[Ni_2(L\text{-}asp)_2(bpe)]\cdot(G)$ with overlapping components along the *a* axis results in the formation of narrow windows in the structure. The van der Waals dimensions of bpe are approximately 12.5 × 6.4 × 3.4 Å. Pyridyl rings of bpe thus fit in the available pores of dimensions 7.9 × 3.3 Å. The windows in $[Ni_2(L\text{-}asp)_2(bpe)]\cdot(G)$ have a cross section of 4.1 × 3.9 Å (*b* × *c* axis). The narrowest part of the bpe ligand has a cross section of approximately 4.9 × 3.4 Å and sits in the windows. Meanwhile, because the $[Ni_2(L\text{-}asp)_2(bpe)]\cdot(G)$ membrane and the $Ni_2(L\text{-}asp)_2(bipy)$ membrane have similar pore volumes (24.8% and 23.1%, respectively), there is no significant difference in their gas permeability. Gas molecules with larger kinetic diameters show a lower permeance. The results of the permeation tests for binary gas mixtures are shown in Fig. 3b. The separation factors of the binary gas mixtures on the $[Ni_2(L\text{-}asp)_2(bpe)]\cdot(G)$ membrane are 24.3, 12.1 and 7.77 for H_2/CO_2, H_2/N_2 and H_2/CH_4, respectively. The separation factor of H_2/CO_2 is much

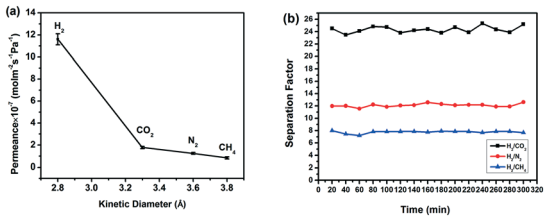

Fig. 3 (a) Permeances of single gases through the $[Ni_2(L\text{-}asp)_2(bpe)]\cdot(G)$ membrane at 298 K as a function of the kinetic diameter; (b) H_2/CH_4, H_2/N_2 and H_2/CO_2 separation factors of $[Ni_2(L\text{-}asp)_2(bpe)]\cdot(G)$ over time.

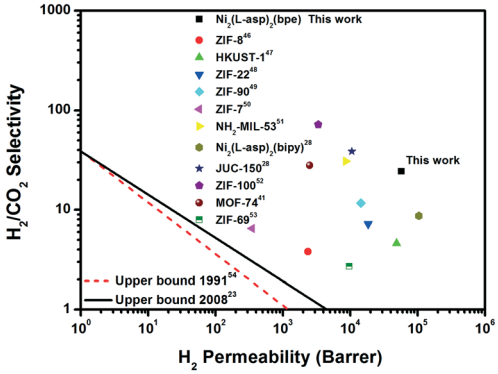

Fig. 4 H_2/CO_2 selectivity as a function of H_2 permeability for $[Ni_2(L\text{-}asp)_2(bpe)]\cdot(G)$ compared with other MOF membranes reported in the literature.[28,41,46–53] The upper bound lines for polymer membranes are drawn according to ref. 23 and 54.

higher than the ideal value. This is due to the strong interaction between CO_2 molecules and the guest bpe molecules, which makes it more difficult for CO_2 molecules than H_2 molecules to pass through the narrow pores. The $[Ni_2(L\text{-}asp)_2(bpe)]\cdot(G)$ membrane shows higher values for both permeability and selectivity for H_2/CO_2 separation in comparison with other membranes, and surpasses the polymer membrane gas separation upper bound of 2008 (Fig. 4), highlighting its potential for application in gas separation. These results indicate that the separation effects of the MOF membranes can be improved by adjusting their pore structure through *in situ* guest molecules.

Conclusions

In summary, a stable $[Ni_2(L\text{-}asp)_2(bpe)]\cdot(G)$ membrane with guest molecules encapsulated in the pores by *in situ* synthesis has been successfully fabricated. The bpe molecules uniformly distributed in the channels not only reduce the window size, but also enhance the interaction between the MOF and CO_2 gas molecules, which makes the membrane suitable for H_2/CO_2 separation. The $[Ni_2(L\text{-}asp)_2(bpe)]\cdot(G)$ membrane demonstrates high H_2 permeance (1.0×10^{-6} mol m^{-2} s^{-1} Pa^{-1}) and provides desired selectivities for binary gas mixtures of H_2/CH_4, H_2/N_2 and H_2/CO_2. Its excellent gas separation performance gives this MOF membrane great potential for applications such as separation, recycling, and reusing H_2 exhausted from steam reforming natural gas. To the best of our knowledge, this is the first report of the *in situ* confinement of free linkers in the channels of a MOF membrane to improve its gas separation properties. It may provide a general method for fine-tuning the pore size of MOF membranes and developing the functional applications of porous MOFs materials.

Acknowledgements

This work was supported by the National Natural Science Foundation of China (21390394, 21571076, 21501198,

 This journal is © The Royal Society of Chemistry 2017

Published on 09 February 2017. Downloaded on 21/03/2017 02:01:20.

21601205, 21371179, 21271117) and the Taishan Scholar Foundation (ts201511019).

Notes and references

1 S. Qiu, M. Xue and G. Zhu, *Chem. Soc. Rev.*, 2014, **43**, 6116–6140.
2 H. Furukawa, K. E. Cordova, M. O'Keeffe and O. M. Yaghi, *Science*, 2013, **341**, 1230444.
3 A. Cadiau, K. Adil, P. M. Bhatt, Y. Belmabkhout and M. Eddaoudi, *Science*, 2016, **353**, 137–140.
4 X. Cui, K. Chen, H. Xing, Q. Yang, R. Krishna, Z. Bao, H. Wu, W. Zhou, X. Dong, Y. Han, B. Li, Q. Ren, M. J. Zaworotko and B. Chen, *Science*, 2016, **353**, 141–144.
5 Y. Yue, P. F. Fulvio and S. Dai, *Acc. Chem. Res.*, 2015, **48**, 3044–3052.
6 F. Luo, C. Yan, L. Dang, R. Krishna, W. Zhou, H. Wu, X. Dong, Y. Han, T. L. Hu, M. O'Keeffe, L. Wang, M. Luo, R. B. Lin and B. Chen, *J. Am. Chem. Soc.*, 2016, **138**, 5678–5684.
7 Q. Gao, J. Xu, D. Cao, Z. Chang and X.-H. Bu, *Angew. Chem., Int. Ed.*, 2016, **55**, 15027–15030.
8 X. Zhao, C. Mao, K. T. Luong, Q. Lin, Q.-G. Zhai, P. Feng and X. Bu, *Angew. Chem., Int. Ed.*, 2015, **55**, 2768–2772.
9 Y. Xiong, Y. Z. Fan, R. Yang, S. Chen, M. Pan, J. J. Jiang and C. Y. Su, *Chem. Commun.*, 2014, **50**, 14631–14634.
10 J.-P. Zhang and X.-M. Chen, *J. Am. Chem. Soc.*, 2012, 6010–6017.
11 P. Q. Liao, D. D. Zhou, A. X. Zhu, L. Jiang, R. B. Lin, J. P. Zhang and X. M. Chen, *J. Am. Chem. Soc.*, 2012, **134**, 17380–17383.
12 D. S. Sholl and R. P. Lively, *Nature*, 2016, **532**, 435–437.
13 J. Y. S. Lin, *Science*, 2016, **353**, 121–122.
14 R. W. Baker, *Membrane Technology and Applications*, John Wiley & Sons, Ltd., Newark, California, 3rd edn, 2012.
15 R. W. Baker, *Ind. Eng. Chem. Res.*, 2002, **41**, 1393–1411.
16 A. F. Ismail and L. I. B. David, *J. Membr. Sci.*, 2001, **193**, 1–18.
17 J. Coronas and J. Santamaría, *Sep. Purif. Methods*, 1999, **28**, 127–177.
18 N. Eng-Poh, D. Chateigner, T. Bein, V. Valtchev and S. Mintova, *Science*, 2012, **335**, 70–73.
19 T. Li, Y. Pan, K.-V. Peinemann and Z. Lai, *J. Membr. Sci.*, 2013, **425**, 235–242.
20 G. Liu, W. Jin and N. Xu, *Angew. Chem., Int. Ed.*, 2016, **55**, 13384–13397.
21 N. Kosinov, J. Gascon, F. Kapteijn and E. J. M. Hensen, *J. Membr. Sci.*, 2016, **499**, 65–79.
22 D. E. Sanders, Z. P. Smith, R. Guo, L. M. Robeson, J. E. McGrath, D. R. Paul and B. D. Freeman, *Polymer*, 2013, **54**, 4729–4761.
23 L. M. Robeson, *J. Membr. Sci.*, 2008, **320**, 390–400.
24 B. D. Freeman, *Macromolecules*, 1999, **32**, 375–380.
25 A. Huang and J. Caro, *Chem. Commun.*, 2010, **46**, 7748–7750.
26 R. W. Baker, *Ind. Eng. Chem. Res.*, 2002, **41**, 1393–1411.
27 H. T. Kwon, H. K. Jeong, A. S. Lee, H. S. An and J. S. Lee, *J. Am. Chem. Soc.*, 2015, **137**, 12304–12311.
28 Z. Kang, M. Xue, L. Fan, L. Huang, L. Guo, G. Wei, B. Chen and S. Qiu, *Energy Environ. Sci.*, 2014, **7**, 4053–4060.
29 A. Huang, Y. Chen, Q. Liu, N. Wang, J. Jiang and J. Caro, *J. Membr. Sci.*, 2014, **454**, 126–132.
30 Y. Ban, Y. Peng, Y. Zhang, H. Jin, W. Jiao, A. Guo, P. Wang, Y. Li and W. Yang, *Microporous Mesoporous Mater.*, 2016, **219**, 190–198.
31 J. R. Li, R. J. Kuppler and H. C. Zhou, *Chem. Soc. Rev.*, 2009, **38**, 1477–1504.
32 P. Hu, Y. Yang, Y. Mao, J. Li, W. Cao, Y. Ying, Y. Liu, J. Lei and X. Peng, *CrystEngComm*, 2015, **17**, 1576–1582.
33 Z. Y. Yeo, P. W. Zhu, A. R. Mohamed and S.-P. Chai, *CrystEngComm*, 2014, **16**, 3072.
34 J. Li, W. Cao, Y. Mao, Y. Ying, L. Sun and X. Peng, *CrystEngComm*, 2014, **16**, 9788–9791.
35 B. Li, Y. Zhang, D. Ma, T. Ma, Z. Shi and S. Ma, *J. Am. Chem. Soc.*, 2014, **136**, 1202–1205.
36 Y.-Z. Chen, Y.-X. Zhou, H. Wang, J. Lu, T. Uchida, Q. Xu, S.-H. Yu and H.-L. Jiang, *ACS Catal.*, 2015, **5**, 2062–2069.
37 Q. Yang, Q. Xu, S.-H. Yu and H.-L. Jiang, *Angew. Chem.*, 2016, **128**, 3749–3753.
38 K. Xu, C. Yuan, J. Caro and A. Huang, *J. Membr. Sci.*, 2016, **511**, 1–8.
39 G. Guan, K. Kusakabe and S. Morooka, *Sep. Sci. Technol.*, 2001, **36**, 2233–2245.
40 A. Huang and J. Caro, *Angew. Chem., Int. Ed.*, 2011, **50**, 4979–4982.
41 N. Wang, A. Mundstock, Y. Liu, A. Huang and J. Caro, *Chem. Eng. Sci.*, 2015, **124**, 27–36.
42 R. Vaidhyanathan, D. Bradshaw, J.-N. Rebilly, J. P. Barrio, J. A. Gould, N. G. Berry and M. J. Rosseinsky, *Angew. Chem., Int. Ed.*, 2006, **45**, 6495–6499.
43 Z. Kang, M. Xue, L. Fan, J. Ding, L. Guo, L. Gao and S. Qiu, *Chem. Commun.*, 2013, **49**, 10569–10571.
44 J. P. Barrio, J.-N. Rebilly, B. Carter, D. Bradshaw, J. Bacsa, A. Y. Ganin, H. Park, A. Trewin, R. Vaidhyanathan, A. I. Cooper, J. E. Warren and M. J. Rosseinsky, *Chem. – Eur. J.*, 2008, **14**, 4521–4532.
45 W. J. Koros, Y. H. Ma and T. Shimidzu, *Pure Appl. Chem.*, 1996, **68**, 1479–1489.
46 K. Huang, Z. Dong, Q. Li and W. Jin, *Chem. Commun.*, 2013, **49**, 10326–10328.
47 J. Nan, X. Dong, W. Wang, W. Jin and N. Xu, *Langmuir*, 2011, **27**, 4309–4312.
48 A. Huang, H. Bux, F. Steinbach and J. Caro, *Angew. Chem., Int. Ed.*, 2010, **49**, 4958–4961.
49 A. Huang, W. Dou and J. Caro, *J. Am. Chem. Soc.*, 2010, **132**, 15562–15564.
50 Y. Li, F. Liang, H. Bux, W. Yang and J. Caro, *J. Membr. Sci.*, 2010, **354**, 48–54.
51 F. Zhang, X. Zou, X. Gao, S. Fan, F. Sun, H. Ren and G. Zhu, *Adv. Funct. Mater.*, 2012, **22**, 3583–3590.
52 N. Wang, Y. Liu, Z. Qiao, L. Diestel, J. Zhou, A. Huang and J. Caro, *J. Mater. Chem. A*, 2015, **3**, 4722–4728.

53 Y. Liu, E. Hu, E. A. Khan and Z. Lai, *J. Membr. Sci.*, 2010, **353**, 36–40.
54 L. M. Robeson, *J. Membr. Sci.*, 1991, **62**, 165–185.
55 S. Basu, M. Maes, A. Cano-Odena, L. Alaerts, D. E. De Vos and I. F. J. Vankelecom, *J. Membr. Sci.*, 2009, **344**, 190–198.

Published on 09 February 2017. Downloaded on 21/03/2017 02:01:20.

This journal is © The Royal Society of Chemistry 2017